Polarizability and magnetoplasmonic properties of magnetic general nanoellipsoids

Nicolò Maccaferri,[1,*] Juan B. González-Díaz,[1] Stefano Bonetti,[2] Andreas Berger,[1] Mikko Kataja,[3] Sebastiaan van Dijken,[3] Josep Nogués,[4] Valentina Bonanni,[5] Zhaleh Pirzadeh,[6] Alexandre Dmitriev,[6] Johan Åkerman,[7] and Paolo Vavassori,[1, 8, 9]

[1]*Nanomagnetism Group, CIC nanoGUNE Consolider, 20018 Donostia-San Sebastián, Spain*
[2]*Department of Physics, Stanford University and Stanford Institute for Materials and Energy Science (SIMES), SLAC National Accelerator Laboratory, CA 94305–2004 Stanford, USA*
[3]*NanoSpin, Department of Applied Physics, Aalto University School of Science, FI-00076 Aalto, Finland*
[4]*Institució Catalana de Recerca i Estudis Avançats (ICREA) and CIN2 (ICN-CSIC) and Universitat Autònoma de Barcelona, Catalan Institute of Nanotechnology (ICN), Campus UAB, 08193 Bellaterra, Spain*
[5]*CNR-ISTM and INSTM, 20133 Milano, Italy*
[6]*Department of Applied Physics, Chalmers University of Technology, 41296 Gothenburg, Sweden*
[7]*Material Physics, Royal Institute of Technology, 16440 Kista, Sweden*
[8]*IKERBASQUE, Basque Foundation for Science, 48011 Bilbao, Spain*
[9]*p.vavassori@nanogune.eu*
**n.maccaferri@nanogune.eu*

Abstract: An approach to compute the polarizability tensor of magnetic nanoparticles having general ellipsoidal shape is presented. We find a surprisingly excellent quantitative agreement between calculated and experimental magneto-optical spectra measured in the polar Kerr configuration from nickel nanodisks of large size (exceeding 100 nm) with circular and elliptical shape. In spite of its approximations and simplicity, the formalism presented here captures the essential physics of the interplay between magneto-optical activity and the plasmonic resonance of the individual particle. The results highlight the key role of the dynamic depolarization effects to account for the magneto-optical properties of plasmonic nanostructures.

OCIS codes: (290.5850) Scattering, particles; (160.1190) Anisotropic optical materials; (160.3820) Magneto-optical materials.

References and links

1. M. Sandtke and L. Kuipers, "Slow guided surface plasmons at telecom frequencies," Nat. Photonics **1**(10), 573–576 (2007).
2. V. E. Ferry, L. A. Sweatlock, D. Pacifici, and H. A. Atwater, "Plasmonic nanostructure design for efficient light coupling into solar cells," Nano Lett. **8**(12), 4391–4397 (2008).
3. S. Lal, S. Link, and N. J. Halas, "Nano-optics from sensing to waveguiding," Nat. Photonics **1**(11), 641–648 (2007).
4. B. Sepúlveda, A. Calle, L. M. Lechuga, and G. Armelles, "Highly sensitive detection of biomolecules with the magneto-optic surface-plasmon-resonance sensor," Opt. Lett. **31**(8), 1085–1087 (2006).
5. G. Armelles, A. Cebollada, A. García-Martín, J. M. García-Martín, M. U. González, J. B. González-Díaz, E. Ferreiro-Vila, and J. F. Torrado, "Magnetoplasmonic nanostructures: systems supporting both plasmonic and magnetic properties," J. Opt. A, Pure Appl. Opt. **11**(11), 114023 (2009).
6. G. Armelles, A. Cebollada, A. García-Martín, and M. U. González, "Magnetoplasmonics: combining magnetic and plasmonic functionalities," Adv. Opt. Mater. **1**, 10–35 (2013).
7. S. Melle, J. L. Menéndez, G. Armelles, D. Navas, M. Vázquez, K. Nielsch, R. B. Wehrspohn, and U. Gösele, "Magneto-optical properties of nickel nanowire arrays," Appl. Phys. Lett. **83**(22), 4547–4549 (2003).
8. V. I. Belotelov, L. L. Doskolovich, and A. K. Zvezdin, "Temporal coherence of photons emitted by single nitrogen-vacancy defect centers in diamond using optical Rabi-oscillations," Phys. Rev. Lett. **98**(7), 077401 (2007).

#184951 - $15.00 USD Received 5 Feb 2013; revised 13 Mar 2013; accepted 28 Mar 2013; published 12 Apr 2013

9. Z. Liu, L. Shi, Z. Shi, X. H. Liu, J. Zi, S. M. Zhou, S. J. Wei, J. Li, X. Zhang, and Y. J. Xia, "Magneto-optical Kerr effect in perpendicularly magnetized Co/Pt films on two-dimensional colloidal crystals," Appl. Phys. Lett. **95**(3), 032502 (2009).
10. G. Ctistis, E. Papaioannou, P. Patoka, J. Gutek, P. Fumagalli, and M. Giersig, "Optical and magnetic properties of hexagonal arrays of subwavelength holes in optically thin cobalt films," Nano Lett. **9**(1), 1–6 (2009).
11. V. Bonanni, S. Bonetti, T. Pakizeh, Z. Pirzadeh, J. Chen, J. Nogués, P. Vavassori, R. Hillenbrand, J. Åkerman, and A. Dmitriev, "Designer magnetoplasmonics with nickel nanoferromagnets," Nano Lett. **11**(12), 5333–5338 (2011).
12. J. Chen, P. Albella, Z. Pirzadeh, P. Alonso-González, F. Huth, S. Bonetti, V. Bonanni, J. Åkerman, J. Nogués, P. Vavassori, A. Dmitriev, J. Aizpurua, and R. Hillenbrand, "Plasmonic nickel nanoantennas," Small **7**(16), 2341–2347 (2011).
13. T. Katayama, Y. Suzuki, H. Awano, Y. Nishihara, and N. Koshizuka, "Enhancement of the magneto-optical Kerr rotation in Fe/Cu bilayered films," Phys. Rev. Lett. **60**(14), 1426–1429 (1988).
14. J. B. González-Díaz, A. García-Martín, J. M. García-Martín, A. Cebollada, G. Armelles, B. Sepúlveda, Y. Alaverdyan, and M. Käll, "Plasmonic Au/Co/Au nanosandwiches with enhanced magneto-optical activity," Small **4**(2), 202–205 (2008).
15. J. B. González-Díaz, B. Sepulveda, A. García-Martín, and G. Armelles, "Cobalt dependence of the magneto-optical response in magnetoplasmonic nanodisks," Appl. Phys. Lett. **97**(4), 043114 (2010).
16. J. C. Banthí, D. Meneses-Rodríguez, F. García, M. U. González, A. García-Martín, A. Cebollada, and G. Armelles, "High magneto-optical activity and low optical losses in metal-dielectric Au/Co/Au-SiO_2 magnetoplasmonic nanodisks," Adv. Mater. **24**(10), OP36–OP41 (2012).
17. V. V. Temnov, G. Armelles, U. Woggon, D. Guzatov, A. Cebollada, A. García-Martín, J. M. García-Martín, T. Thomay, A. Leitenstorfer, and R. Bratschitsch, "Active magneto-plasmonics in hybrid metal–ferromagnet structures," Nat. Photonics **4**(2), 107–111 (2010).
18. G. Armelles, J. B. González-Díaz, A. García-Martín, J. M. García-Martín, A. Cebollada, M. Ujué González, S. Acimovic, J. Cesario, R. Quidant, and G. Badenes, "Localized surface plasmon resonance effects on the magneto-optical activity of continuous Au/Co/Au trilayers," Opt. Express **16**(20), 16104–16112 (2008).
19. F. Wang, A. Chakrabarty, F. Minkowski, K. Sun, and Q. Wei, "Polarization conversion with elliptical patch nanoantennas," Appl. Phys. Lett. **101**(2), 023101 (2012).
20. J. B. González-Díaz, A. García-Martín, G. Armelles, D. Navas, M. Vázquez, K. Nielsch, R. B. Wehrspohn, and U. Gösele, "Enhanced magneto-optics and size effects in ferromagnetic nanowire arrays," Adv. Mater. **19**(18), 2643–2647 (2007).
21. J. B. González-Díaz, J. M. García-Martín, A. García-Martín, D. Navas, A. Asenjo, M. Vázquez, M. Hernández-Vélez, and G. Armelles, "Plasmon-enhanced magneto-optical activity in ferromagnetic membranes," Appl. Phys. Lett. **94**(26), 263101 (2009).
22. P. K. Jain, Y. Xiao, R. Walsworth, and A. E. Cohen, "Surface plasmon resonance enhanced magneto-optics (SuPREMO): Faraday rotation enhancement in gold-coated iron oxide nanocrystals," Nano Lett. **9**(4), 1644–1650 (2009).
23. E. Th. Papaioannou, V. Kapaklis, P. Patoka, M. Giersig, P. Fumagalli, A. García-Martín, E. Ferreiro-Vila, and G. Ctistis, "Magneto-optic enhancement and magnetic properties in Fe antidot films with hexagonal symmetry," Phys. Rev. B **81**(5), 054424 (2010).
24. L. Wang, C. Clavero, Z. Huba, K. J. Carroll, E. E. Carpenter, D. Gu, and R. A. Lukaszew, "Plasmonics and enhanced magneto-optics in core-shell Co-Ag nanoparticles," Nano Lett. **11**(3), 1237–1240 (2011).
25. M. Rubio-Roy, O. Vlasin, O. Pascu, J. M. Caicedo, M. Schmidt, A. R. Goñi, N. G. Tognalli, A. Fainstein, A. Roig, and G. Herranz, "Magneto-optical enhancement by plasmon excitations in nanoparticle/metal structures," Langmuir **28**(24), 9010–9020 (2012).
26. D. R. Fredkin and I. D. Mayergoyz, "Resonant behavior of dielectric objects (electrostatic resonances)," Phys. Rev. Lett. **91**(25), 253902 (2003).
27. I. D. Mayergoyz, D. R. Fredkin, and Z. Zhang, "Electrostatic (plasmon) resonances in nanoparticles," Phys. Rev. B **72**(15), 155412 (2005).
28. A. F. Stevenson, "Electromagnetic scattering by an ellipsoid in the third approximation," J. Appl. Phys. **24**(9), 1143–1151 (1953).
29. A. Wokaun, J. P. Gordon, and P. F. Liao, "Radiation damping in surface-enhanced Raman scattering," Phys. Rev. Lett. **48**(14), 957–960 (1982).
30. M. Meier and A. Wokaun, "Enhanced fields on large metal particles: dynamic depolarization," Opt. Lett. **8**(11), 581–583 (1983).
31. M. Meier, A. Wokaun, and P. F. Liao, "Enhanced fields on rough surfaces: dipolar interactions among particles of sizes exceeding the Rayleigh limit," J. Opt. Soc. Am. B **2**(6), 931–949 (1985).
32. A. Moroz, "Depolarization field of spheroidal particles," J. Opt. Soc. Am. B **26**(3), 517–527 (2009).
33. A. Lakhtakia, "Rayleigh scattering by bianisotropic ellipsoid in a biisotropic medium," Int. J. Electron. **71**(6), 1057–1062 (1991).
34. A. Lakhtakia, "Strong and weak forms of the method of moments and the coupled dipole method for scattering of time-harmonic electromagnetic fields," Int. J. Mod. Phys. C **3**(3), 583–603 (1992).

#184951 - $15.00 USD Received 5 Feb 2013; revised 13 Mar 2013; accepted 28 Mar 2013; published 12 Apr 2013

35. R. Landauer, “The electrical resistance of binary metallic mixtures,” J. Appl. Phys. **23**(7), 779–784 (1952).
36. D. Stroud, “Generalized effective-medium approach to the conductivity of an inhomogeneous material,” Phys. Rev. B **12**(8), 3368–3373 (1975).
37. M. Schubert, T. E. Tiwald, and J. A. Woollam, “Explicit solutions for the optical properties of arbitrary magneto-optic materials in generalized ellipsometry,” Appl. Opt. **38**(1), 177–187 (1999).
38. J. Zak, E. R. Mook, C. Liu, and S. D. Bader, “Universal approach to magneto-optics,” J. Magn. Magn. Mater. **89**(1–2), 107–123 (1990).
39. Š. Višňovský, R. Lopusnik, M. Bauer, J. Bok, J. Fassbender, and B. Hillebrands, “Magnetooptic ellipsometry in multilayers at arbitrary magnetization,” Opt. Express **9**(3), 121–135 (2001).
40. H. Fredriksson, Y. Alaverdyan, A. Dmitriev, C. Langhammer, D. S. Sutherland, M. Zäch, and B. Kasemo, “Hole–mask colloidal lithography,” Adv. Mater. **19**(23), 4297–4302 (2007).
41. R. A. de la Osa, J. F. Saiz, M. Moreno, P. Vavassori, and A. Berger, “Transverse magneto-optical effects in nanoscale disks,” Phys. Rev. B **85**(6), 064414 (2012).
42. D. Y. K. Ko and J. C. Inkson, “Matrix method for tunnelling in heterostructures: resonant tunnelling in multilayer systems,” Phys. Rev. B **38**(14), 9945–9951 (1988).
43. D. M. Whittaker and I. S. Culshaw, “Scattering-matrix treatment of patterned multilayer photonic structures,” Phys. Rev. B **60**(4), 2610–2618 (1999).
44. B. Caballero, A. Garcia Martin, and J. C. Cuevas, “Generalized scattering-matrix approach for magneto-optics in periodically patterned multilayer systems,” Phys. Rev. B **85**(24), 245103 (2012).
45. Z. J. Yang and M. R. Scheinfein, “Combined three-axis surface magneto-optical Kerr effects in the study of surface and ultrathin-film magnetism,” J. Appl. Phys. **74**(11), 6810–6823 (1993).
46. H. Kang and G. W. Milton, “Solutions to the Pólya–Szegö conjecture and the weak Eshelby conjecture,” Arch. Ration. Mech. Anal. **188**(1), 93–116 (2008).
47. W. L. Bragg and A. B. Pippard, “The form birefringence of macromolecules,” Acta Crystallogr. **6**(11), 865–867 (1953).
48. One should consider also the phase difference due to the incoming light hitting a finite size body. There are several ways to account for this phase difference reported in literature [30, 32, 49]. Although, we verified that inclusion of these corrections have negligible effects, and therefore for sake of clarity we neglect them. We point out, in addition, that for the particular geometry used in our experiments, namely perpendicular incidence over flat disks, this phase difference effects are rigorously zero.
49. H. Kuwata, H. Tamaru, K. Esumi, and K. Miyano, “Resonant light scattering from metal nanoparticles: practical analysis beyond Rayleigh approximation,” Appl. Phys. Lett. **83**(22), 4625–4627 (2003).
50. K. L. Kelly, E. Coronado, L. L. Zhao, and G. C. Schatz, “The optical properties of metal nanoparticles: the influence of size, shape, and dielectric environment,” J. Phys. Chem. B **107**(3), 668–677 (2003).
51. H. C. van de Hulst, *Light Scattering by Small Particles* (Wiley, 1957).
52. C. F. Bohren and D. R. Huffman, *Absorption and Scattering of Light by Small Particles* (Wiley, 1983).
53. V. G. Farafonov, V. B. Il’in, and M. S. Prokop’eva, “Light scattering by homogeneous and multilayer ellipsoids in the quasi-static approximation,” Opt. Spectrosc. **92**(4), 567–576 (2002).
54. V. Myroshnychenko, J. Rodríguez-Fernández, I. Pastoriza-Santos, A. M. Funston, C. Novo, P. Mulvaney, L. M. Liz-Marzán, and F. J. García de Abajo, “Modelling the optical response of gold nanoparticles,” Chem. Soc. Rev. **37**(9), 1792–1805 (2008).
55. L. Landau and E. M. Lifschitz, *Electrodynamics of Continuous Media*, (Ed. Pergamon, 1984)
56. For a proper comparison, it is necessary to establish the association between D_x, D_y and D_z and $D_{\parallel}$ and $D_{\perp}$ from Moroz. Based on the definitions of the eccentricities given in the text, our prolate profile is characterized by $a_x = a_z < a_y$, so D_x and D_z are equivalent to $D_{\parallel}$ and D_y to $D_{\perp}$, whereas the oblate profile is characterized by $a_x = a_z < a_y$, so that D_x is equivalent this time to $D_{\perp}$, while D_y and D_z to $D_{\parallel}$.
57. http://www.nanogune.eu/en/research/nanomagnetism/polarizability-calculator/.
58. L. A. Golovan, S. V. Zabotnov, V. Yu. Tinoshenko, and P. K. Kashkarov, “Consideration for the dynamic depolarization in the effective-medium model for description of optical properties for anisotropic nanostructured semiconductors,” Semiconductors **43**(2), 218–222 (2009).
59. J. C. Maxwell-Garnett, “Colours in metal glasses and in metallic films,” Philos. Trans. R. Soc. Lond. B Biol. Sci. **203**(359-371), 385–420 (1904).
60. A. Lakhtakia, “General theory of Maxwell-Garnett model for particulate composites with bi-isotropic host materials,” Int. J. Electron. **73**(6), 1355–1362 (1992).
61. M. Abe, “Derivation of non-diagonal effective dielectric-permeability tensors for magnetized granular composites,” Phys. Rev. B **53**(11), 7065–7075 (1996).
62. M. Abe and T. Suwa, “Surface plasma resonance and magneto-optical enhancement in composites containing multicore-shell structured nanoparticles,” Phys. Rev. B **70**(23), 235103 (2004).
63. P. M. Hui and D. Stroud, “Theory of Faraday rotation by dilute suspensions of small particles,” Appl. Phys. Lett. **50**(15), 950–952 (1987).
64. T. K. Xia, P. M. Hui, and D. Stroud, “Theory of Faraday rotation in granular magnetic materials,” J. Appl. Phys. **67**(6), 2736–2741 (1990).
65. M. J. Freiser, “A survey of magnetooptic effects,” IEEE Trans. Magn. **4**(2), 152–161 (1968).

#184951 - $15.00 USD Received 5 Feb 2013; revised 13 Mar 2013; accepted 28 Mar 2013; published 12 Apr 2013

66. This value for the embedding medium refractive index is chosen since the nano-disks embedded in air have one side in contact with the glass substrate. In the calculation we don't account for the dispersion in the disks size, and we assume that the diameters are the average ones, although the dispersion in diameter can be easily included in Eq. (6) (following Ref. [62]), if required.
67. S. A. Maier, *Plasmonics: Fundamentamentals and Applications*, (Springer, 2007).
68. V. Giannini, A. I. Fernández-Domínguez, S. C. Heck, and S. A. Maier, "Plasmonic nanoantennas: fundamentals and their use in controlling the radiative properties of nanoemitters," Chem. Rev. **111**(6), 3888–3912 (2011).
69. C. Fourn and C. Brosseau, "Electrostatic resonances of heterostructures with negative permittivity: homogenization formalisms versus finite-element modeling," Phys. Rev. E Stat. Nonlin. Soft Matter Phys. **77**(1), 016603 (2008).
70. A. Mejdoubi and C. Brosseau, "Intrinsic electrostatic resonances of heterostructures with negative permittivity from finite-element calculations: application to core-shell inclusions," J. Appl. Phys. **102**(9), 094104 (2007).
71. P. Vavassori, "Polarization modulation technique for magneto-optical quantitative vector magnetometry," Appl. Phys. Lett. **77**(11), 1605–1607 (2000).
72. G. S. Krinchik and V. A. Artem'ev, "Magneto-optical properties of Ni, Co, and Fe in the ultraviolet visible, and infrared parts of the spectrum," Sov. Phys. JTEP **26**(6), 1080–1085 (1968).
73. Š. Višňovský, V. Pařízek, M. Nývlt, P. Kielar, V. Prosser, and R. Krishnan, "Magneto-optical Kerr spectra of nickel," J. Magn. Magn. Mater. **127**(1–2), 135–139 (1993).
74. S. Albaladejo, R. Gómez-Medina, L. S. Froufe-Pérez, H. Marinchio, R. Carminati, J. F. Torrado, G. Armelles, A. García-Martín, and J. J. Sáenz, "Radiative corrections to the polarizability tensor of an electrically small anisotropic dielectric particle," Opt. Express **18**(4), 3556–3567 (2010).

1. Introduction

Electromagnetic scattering from metallic nanometer-scale particles is currently a topic of huge interest, which is being investigated both theoretically and experimentally for the purpose of understanding the underlying physics and investigate novel near- and far-field effects that could be exploited in a broad variety of applications ranging from novel nano-optical devices for optical communications [1] to energy harvesting [2] and optical biosensors with enhanced sensitivity [3, 4]. The vast majority of these studies are performed on noble-metal nanostructures and are focused on the effects on the scattered field due to the nano-confinement of electric fields caused by the excitation of localized plasmon resonances (LPRs) in single nanoparticles, which are collective oscillations of free conductive electron plasma resonantly excited by the electric field of the impinging light.

More recently, the research efforts moved to the study of magnetoplasmonic nanostructures, viz., nanostructures that combine magnetic and plasmonic functionalities [5, 6], since they could be the building block of a new class of magnetically controllable optical nanodevices for future biotechnological and optoelectronic applications. This new research direction has brought forward numerous studies of the effects arising from the mutual interplay between magneto-optical (MO) activity and light-matter coupling in spatially confined geometries [7–11]. Since plasma oscillations in ferromagnetic materials typically exhibit a stronger damping than in noble metals [12], a common strategy to overcome this excess damping was to develop hybrid structures consisting of noble metals and ferromagnetic materials, where the noble metal increases the plasmonic response [13–18].

However, very recently, it was shown how the concerted action of LPRs in single nanoparticles and magnetization can be exploited to actively manipulate the reflected light's polarization (i.e., to induce and control Kerr rotation/ellipticity reversal) of pure ferromagnetic nanostructures beyond what is offered by intrinsic material properties [11]. While most of the investigations carried out before were focused on the achievement of substantial enhancement of magneto-optical Kerr effect (MOKE) or Faraday rotation [19–25], [11] shifted the paradigm of research on magnetoplasmonic functional materials by exploiting the phase tunability of the optical polarizability due to the excitation of LPRs in single nanoparticles and the simultaneous presence of magneto-optical activity in the same ferromagnetic nanostructures. Bonanni et al. showed that anisotropic polarizability of the nanostructures due to their shape (circular and elliptical nanodisks) is one of the key parameters and, together with their size and MO properties, affects their magneto-optical response.

#184951 - $15.00 USD Received 5 Feb 2013; revised 13 Mar 2013; accepted 28 Mar 2013; published 12 Apr 2013

Driven by this recent turn of the research direction in pure ferromagnetic plasmonic nanoparticles, we describe here a formalism to compute the polarizability, as well as far-field MO spectra, of large magnetic ellipsoidal nanoelements, i.e., exceeding the Rayleigh limit (electrostatic regime [26, 27]). We demonstrate that our approach can be applied to real samples of optically non-interacting flat disks with circular and elliptical sections, and size up to a few hundred nanometers. This is a particular relevant case since for disk-shaped magnetic nanostructures in this range of size, LPRs in single nanoparticles fall in the visible spectral region [11, 12].

The problem of the light scattering from a general ellipsoid was treated by Stevenson in the early 50s [28] and in the 80s by Meier, Wokaun, and Liao using a Long Wavelength Approximation (LWA) for isotropic nanoparticles exceeding the Rayleigh limit [29–31] and recently solved analytically by Moroz for the computation of the polarizability of non-magnetic spheroidal particles (oblate and prolate ellipsoids) [32]. The optical response of bi-anisotropic ellipsoids has been already addressed by Lakhtakia [33, 34].

The aim of this work is to determine the optical response of a generalized ellipsoid including also the optical anisotropy arising from the magneto-optical properties of a magnetic material. To this purpose we extend the LWA method, and provide the relevant guidelines of how to compute in a simple way the polarizability tensor of a magnetic nanoellipsoid including radiative, static, and dynamic depolarization factors. We show that the latter is the key factor accounting for the role of the shape and size of the single nanoparticle in determining its optical and MO responses when its dimensions become comparable to the wavelength of the impinging light. In this case the quasi-static (or electrostatic) approximation normally used is no more valid and consequently one has to consider also field retardation effects and energy losses occurring inside the nanoparticle. This knowledge is crucial in magnetoplasmonic devices design, since it enables the accurate control of the position of the LPRs and its dependence on the particle orientation with respect to the oscillation direction of the electric field of the impinging light. We also show that the excitation of a LPR strongly affects the MO activity of the particle. For the calculation of the far-field optical and MO spectral responses we first employ the polarizability of a single nanoparticle computed with our approach in a standard effective medium approximation (EMA) [35, 36], used to model the ensemble of optically non-interacting magnetic ellipsoidal particles embedded in a medium as an effective composite film. Then we apply the Transfer Matrix Method (TMM) [37–39], for the calculation of the optical and magneto-optical far-field responses of multi-layered systems, viz., in our case, the effective magnetic film, calculated with the EMA on a glass substrate. Finally, we compare the results of our modelling against the experimental far-field optical and MO spectra, the latter measured in the Polar-MOKE (P-MOKE) configuration from Ni nanodisks, made with Hole-Mask Colloidal Lithography technique [40]. The disks have diameters in the 100 nm range, with circular and elliptical sections, and are distributed on a glass substrate with an average inter-particle distance exceeding 1.5 times the diameter, viz., they do not optically interact. The excellent agreement obtained between calculated and measured spectra using the sizes and densities of the disks determined by scanning electron microscopy (SEM) imaging of the samples and the optical and MO constants of glass and Ni taken from the literature, viz., without adjustable parameters, indicates that in spite of its apparent simplicity, modelling of disks by generalized ellipsoids captures the essential physics of the interplay between magneto-optical activity and light-matter coupling in such spatially confined geometries. Besides the physics relevance of this result, on a more practical footing, we provide the continuously growing magnetoplasmonic community of an approximate method, which is sufficiently accurate for optical non-interacting nanoparticles and it can be used in alternative to more accurate and exact numerical approaches as the Discrete Dipole Approximation (DDA) [41] or the Scattering-Matrix Method [42–44].

#184951 - $15.00 USD Received 5 Feb 2013; revised 13 Mar 2013; accepted 28 Mar 2013; published 12 Apr 2013

2. Theory

To obtain the polarizability tensor $\tilde{\alpha}$ of a general ellipsoidal magnetic nanoparticle with semi-axes a_x, a_y and a_z (see Fig. 1), let's consider the particle embedded in a non-magnetic host medium described by a diagonal dielectric tensor $\tilde{\varepsilon}_1 = \varepsilon_1 \tilde{I}$, where $\tilde{I}$ is the identity matrix.

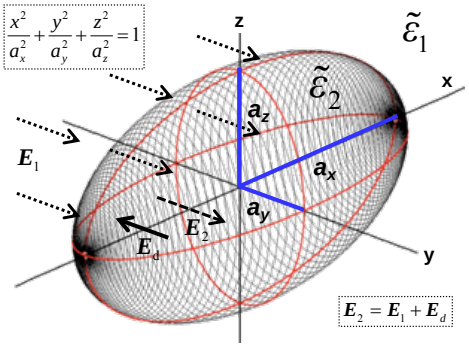

Fig. 1. Scheme of a general ellipsoid embedded in a non-magnetic host medium. The ellipsoid is under the influence of an acting field $\boldsymbol{E}_1$, and, due to the induced dipole moments, the electric field $\boldsymbol{E}_2$ inside it changes.

Given the magnetic character of the nanoparticle, its dielectric susceptibility tensor, in the presence of an external magnetic field high enough to saturate the particle magnetization, presents non-diagonal components. For the sake of direct comparison with magneto-optical experiments, it is customary to use the s-p linearly polarized light base. Thus, including terms which are of first order in $\hat{\boldsymbol{m}} = m_x + m_y + m_z$, the unit magnetization vector expressed in terms of the Euler's angles director cosines, it can be represented, for a material having cubic symmetry, by a non-diagonal, anti-symmetric, tensor $\tilde{\varepsilon}_2$ [45]:

$$\tilde{\varepsilon}_2 = \begin{pmatrix} \varepsilon_2 & -iQ\varepsilon_2 m_z & iQ\varepsilon_2 m_y \\ iQ\varepsilon_2 m_z & \varepsilon_2 & -iQ\varepsilon_2 m_x \\ -iQ\varepsilon_2 m_y & iQ\varepsilon_2 m_x & \varepsilon_2 \end{pmatrix}$$

where Q is the Voigt magneto-optical constant.

Let's consider an incident plane electromagnetic wave $\boldsymbol{E}(\boldsymbol{r}, t) = \boldsymbol{E}_1 e^{[i(\boldsymbol{k}\cdot\boldsymbol{r}-\omega t)]}$ impinging on the particle. Following [30, 32], we initially neglect the space variation of $\boldsymbol{E}(\boldsymbol{r}, t)$ over the nanoparticle volume, viz., $\boldsymbol{E}(\boldsymbol{r}, t) = \boldsymbol{E}_1 e^{-i\omega t}$. Under this assumption and through the weak Eshelby conjecture, the internal field $\boldsymbol{E}_2$ and therefore the induced polarization $\boldsymbol{P}$ can be assumed uniform over the volume of a particle of ellipsoidal shape [46]. Following Bragg and Pippard [47] we can write:

$$\boldsymbol{P} = (\tilde{\varepsilon}_2 - \tilde{\varepsilon}_1)\boldsymbol{E}_2 = (\tilde{\varepsilon}_2 - \tilde{\varepsilon}_1)(\boldsymbol{E}_1 + \boldsymbol{E}_d) = \tilde{\alpha}\boldsymbol{E}_1 \qquad (1)$$

where the polarizability $\tilde{\alpha}$ can be obtained once the depolarization field $\boldsymbol{E}_d$ is determined. Strictly speaking, Eq. (1) is valid only for very small ellipsoidal particles, for which the the external field can be assumed uniform. According to Meier and Wokaun [30] and using Eq. (1), the finite size of the particle can be approximately accounted for in the calculation of $\boldsymbol{E}_d$. This is done by assigning a dipole moment $d\boldsymbol{p} = \boldsymbol{P}dV$ to each volume element dV of the ellipsoid and calculating the retarded depolarization field $d\boldsymbol{E}_d$ generated by $d\boldsymbol{p}$ in the center of

#184951 - $15.00 USD Received 5 Feb 2013; revised 13 Mar 2013; accepted 28 Mar 2013; published 12 Apr 2013

such an ellipsoid [48]. Passing in spherical coordinates and integrating over all the particle volume we obtain the following expression [32]:

$$\boldsymbol{E}_d = \int d\boldsymbol{E}_d = \int \left(\frac{3\hat{\boldsymbol{u}}(\boldsymbol{P}\cdot\hat{\boldsymbol{u}}) - P}{r^3} + i\frac{2\boldsymbol{P}}{3}k^3 + \frac{\hat{\boldsymbol{u}}(\boldsymbol{P}\cdot\hat{\boldsymbol{u}})}{2r}k^2 \right) dV \tag{2}$$

being k the light wave vector modulus, r the distance from the center of the ellipsoid, and $\hat{\boldsymbol{u}}$ the unit vector having the direction of $\boldsymbol{r}$. The depolarization field $\boldsymbol{E}_d$ in the center of the ellipsoid given by Eq. (2) is assumed to be the average depolarization field inside the particle. The first term in the integral in Eq. (2) corresponds to the static depolarization due to a uniform $\boldsymbol{E}_1$ and accounts for the shape of the nanoparticle. This term is the only one usually considered for cases in which the wavelength of the impinging light λ is much larger than the characteristic dimensions of the nanoparticle (Rayleigh scattering limit, known also as quasi-static or electrostatic regime). The second term is the radiative reaction due to the recoil force, known also as the Abraham–Lorentz force, acting on an oscillating dipole emitting electromagnetic radiation [29]. The integration of this term is straightforward and yields to $i(2/3)k^3\mathrm{V}\boldsymbol{P}$. The third term in the integral is the so called dynamic depolarization and arises from de-phasing of the radiation emitted by different points in the ellipsoid. This term is considered negligible, and therefore normally discarded, for particles size in the Rayleigh (electrostatic) regime ($r \ll \lambda$ and $r \ll \xi$, where r is the radius or any semi-axis of the ellipsoid and ξ is the skin depth). However, considering this term for larger particles, whose characteristic dimensions are no longer in the Rayleigh regime as those we aim at dealing with in this work, is of key importance. The inclusion of this term complicates substantially the calculation of the integral in Eq. (2). It can be shown that Eq. (2) can be cast in the following, most convenient, tensorial form by factorizing out the polarization $\boldsymbol{P}$:

$$\boldsymbol{E}_d = -\tilde{\varepsilon}_1^{-1}\left(\tilde{L} - i\frac{k^3 V}{6\pi}\tilde{I} - \frac{k^2 V}{4\pi}\tilde{D} \right)\cdot \boldsymbol{P} \tag{3}$$

where $\tilde{L} = diag(L_x, L_y, L_z)$ and $\tilde{D} = diag(D_x/a_x, D_y/a_y, D_z/a_z)$ are the static and dynamic geometrical tensors, and $V = [(4\pi/3)a_x a_y a_z]$ is the particle volume.

The static tensor has been calculated in many previous works [50–54]. As stated above, this tensor is related to the shape of the ellipsoids with semi-axes a_x, a_y and a_z and its elements can be calculated as follows [55]

$$L_i = \frac{a_i a_j a_k}{2}\int_0^\infty \left(q + a_i^2\right)^{-\frac{3}{2}} \left(q + a_j^2\right)^{-\frac{1}{2}} \left(q + a_k^2\right)^{-\frac{1}{2}} dq \tag{4}$$

where $i = x, y, z$ with $j,k \neq i$, and $L_{ij} = 0$ if $i \neq j$. The integrals in Eq. (4) have to be computed numerically for a general magnetic ellipsoids. The second term in the expression of $\boldsymbol{E}_d$, the radiative reaction tensor $(i/6\pi)k^3\mathrm{V}\tilde{\mathrm{I}}$, within our approximation is determined only by the time variation of the electric field and is simply proportional to the volume V of the particle. The third term is the most complicated to calculate and its explicit expression has been derived, in the LWA framework, only for the particular cases of a sphere [30] as well as of prolate and oblate spheroids [32], since only in these cases it admit an analytical solution. In the more general case treated here, the diagonal elements of this tensor have to be calculated numerically. In order to facilitate the implementation of such calculations, we devised their expressions in cylindrical coordinates:

#184951 - $15.00 USD Received 5 Feb 2013; revised 13 Mar 2013; accepted 28 Mar 2013; published 12 Apr 2013

$$D_x = \frac{3a_x}{4\pi}\int_0^1 dz'\int_0^{2\pi} d\theta\int_0^{\sqrt{1-z'^2}} \frac{\rho^2(2a_x^2\cos^2\theta + a_y^2\sin^2\theta) + a_z^2 z'^2}{[\rho^2(a_x^2\cos^2\theta + a_y^2\sin^2\theta) + a_z^2 z'^2]^{3/2}}\rho d\rho$$

$$D_y = \frac{3a_y}{4\pi}\int_0^1 dz'\int_0^{2\pi} d\theta\int_0^{\sqrt{1-z'^2}} \frac{\rho^2(a_x^2\cos^2\theta + 2a_y^2\sin^2\theta) + a_z^2 z'^2}{[\rho^2(a_x^2\cos^2\theta + a_y^2\sin^2\theta) + a_z^2 z'^2]^{3/2}}\rho d\rho \qquad (5)$$

$$D_z = \frac{3a_z}{4\pi}\int_0^1 dz'\int_0^{2\pi} d\theta\int_0^{\sqrt{1-z'^2}} \frac{\rho^2(a_x^2\cos^2\theta + a_y^2\sin^2\theta) + 2a_z^2 z'^2}{[\rho^2(a_x^2\cos^2\theta + a_y^2\sin^2\theta) + a_z^2 z'^2]^{3/2}}\rho d\rho$$

The integrals in Eqs. (4) and (5) are valid for a general magnetic ellipsoid in an isotropic embedding medium. The calculated dynamic and static terms for a general ellipsoid are depicted in Figs. 2(a)-2(c) and Figs. 2(d)-2(f), respectively, where we show the value of these tensors elements for all possible aspect ratios that a general ellipsoid may present. The intensity plots show these values as a function of the relative eccentricities in between semi-axes a_x and a_y (abscissa), i.e. $e_1 = \sqrt{(a_y^2 - a_x^2)/a_y^2}$, and in between semi-axes a_x and a_z (ordinate), i.e. $e_2 = \sqrt{(a_z^2 - a_x^2)/a_z^2}$.

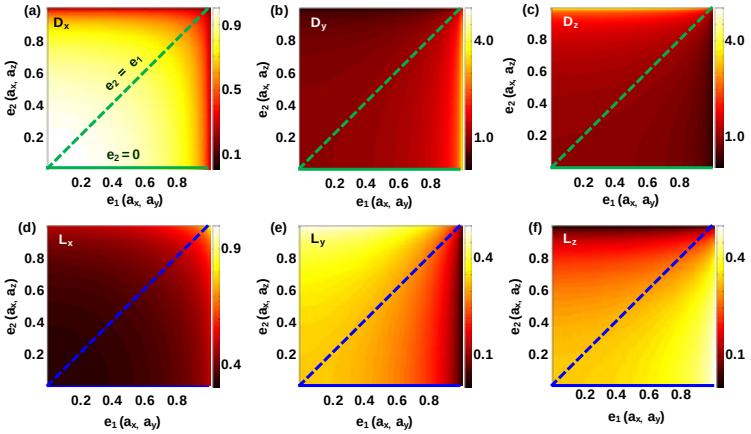

Fig. 2. Numerical calculation of the dynamic and static terms of the depolarization field as a function of the ellipsoid aspect ratio. The abscissa and ordinate shows the relative eccentricity in between axes a_x and a_y, and between a_x, and a_z, respectively for (a) D_x, (b) D_y, (c) D_z, (d) L_x, (e) L_y , and (f) L_z.

The semi-axis a_x is fixed to 1 for simplicity. The color scale presents the D_i or the L_i term value. The continuous and dashed green and blue lines correspond to the particular cases of prolate and oblate spheroid, respectively. With the value 0 representing the absence of eccentricity, it is easy to see that the origin of coordinates corresponds to the perfect sphere, for which all D_i values are equal to 1.

To check the accuracy of the numerical calculations, in Fig. 3 we plot the behavior of the dynamical and static factors for particular ellipsoid transformations, namely, the cases of prolate and oblate spheroids. In this way we can make a direct comparison to the analytical results derived by Moroz for these two particular cases (see Fig. 2 of [32].). The comparison shows that our calculations reproduce exactly the analytical results obtained by Moroz [56]. It can be also noted that the dependence of the dynamic depolarization factors on the eccentricity of the ellipsoid along any of the principal axes is not linear. This has a direct repercussion on the shift of the wavelength position of the nanoparticle plasmon resonance changing its size and shape.

#184951 - $15.00 USD Received 5 Feb 2013; revised 13 Mar 2013; accepted 28 Mar 2013; published 12 Apr 2013

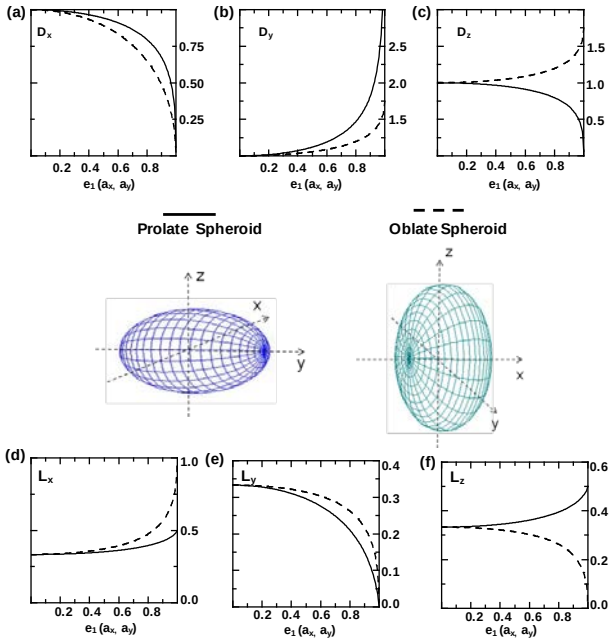

Fig. 3. (a) D_x, (b) D_y, (c) D_z, (d) L_x, (e) L_y , and (f) L_z. The continuous and dashed lines correspond to the dynamic and static components for the particular cases of prolate and oblate spheroids, oriented as pictured in between the plots of the two tensors elements.

Once the depolarization field $\boldsymbol{E}_d$ is calculated including the static, dynamic and radiative corrections, it is straightforward to obtain the polarizability of a nanoparticle from Eq. (1) [57]:

$$\tilde{\alpha} = \left(\tilde{\varepsilon}_2 - \tilde{\varepsilon}_1\right)\left[\tilde{I} + \left(\tilde{L} - \frac{k^2 V}{4\pi}\tilde{D} - i\frac{k^3 V}{6\pi}\tilde{I}\right)\left(\tilde{\varepsilon}_2 - \tilde{\varepsilon}_1\right)\tilde{\varepsilon}_1^{-1}\right]^{-1} \tag{6}$$

This expression derived here is similar to that found in other studies, like [58], but with the particularity of being rigorously tensorial. In this form Eq. (6) can be applied also to calculate the MO response of a general ellipsoidal magnetic particle by using the appropriate anti-symmetric tensor $\tilde{\varepsilon}_2$. From Eq. (6) one can now apply any suitable method, appropriate for the particular case under consideration, to obtain the far-fields and, consequently, the MO response of an ensemble of ellipsoidal nanoparticles.

Since we aim at comparing the predictions of our approach with experiments preformed on samples where the nanoparticles are distributed with a low concentration (up to 15% and so they are optically non-interacting) over a glass substrate, we decided to use the Maxwell-Garnett (MG) Effective Medium Approximation (EMA) [59, 60] for such a calculation. This method models the nanoparticles in the embedding medium, a mix of air and glass in our case, as a homogeneous film described by an effective dielectric tensor. This approximation is known to provide an accurate description of the reflected field if the nanoparticles are small compared to the wavelength of the incoming light, and do not interact among each other. The formalism to obtain such effective dielectric tensor of a magneto-optically active system follows that developed by Abe and Suwa [61, 62] and is based on the earliest works of Hui and Stroud [63] and Xia, Hui and Stroud [64]. In the case of non-spheroidal elements, we furthermore consider the particles all oriented in the same spatial direction, as they actually are in our samples. Then, following [62] and using Eq. (6), the effective dielectric permittivity tensor is obtained as:

#184951 - $15.00 USD Received 5 Feb 2013; revised 13 Mar 2013; accepted 28 Mar 2013; published 12 Apr 2013

$$\tilde{\varepsilon}_{eff} = \tilde{\varepsilon}_1 + f\left(\tilde{\varepsilon}_2 - \tilde{\varepsilon}_1\right)\left[\tilde{I} + (1-f)\left(\tilde{L} - \frac{k^2 V}{4\pi}\tilde{D} - i\frac{k^3 V}{6\pi}\tilde{I}\right)\left(\tilde{\varepsilon}_2 - \tilde{\varepsilon}_1\right)\tilde{\varepsilon}_1^{-1}\right]^{-1} \qquad (7)$$

In order to address the relevance of the dynamic terms in Eq. (7) we consider a system of Ni spheres embedded in air. Figures 4(a) and 4(b) display the diagonal real and imaginary of ε_{eff}^{xx} ($\mathrm{Re}(\varepsilon_{eff}^{xx})$ and $\mathrm{Im}(\varepsilon_{eff}^{xx})$) calculated for a concentration of 10% and varying the radius of such spheres from 5 to 20 nm (r = a_x = a_y = a_z), as functions of the wavelength in the visible (VIS) and near infrared (NIR) regions. If we don't include the dynamical terms, $\mathrm{Re}(\varepsilon_{eff}^{xx})$ and $\mathrm{Im}(\varepsilon_{eff}^{xx})$ are unaffected by the change of particles dimension (red line in the Figs. 4(a)-4(b)) since the static term accounts only for the shape. Once the dynamic terms are included, $\mathrm{Re}(\varepsilon_{eff}^{xx})$ and $\mathrm{Im}(\varepsilon_{eff}^{xx})$ display a size dependence. The plots in Figs. 4(a) and 4(b) show that for particle radius larger than 10 nm the dynamic terms begin to have a noticeable effect in determining the ε_{eff}^{xx} of the system, especially in the VIS spectral region. In Figs. 4(c) and 4(d) we plot the calculated $\mathrm{Re}(\varepsilon_{eff}^{xx})$ and $\mathrm{Im}(\varepsilon_{eff}^{xx})$, for a system of Ni spheres with r = 20 nm embedded in air, and for different concentrations in the range up to 15%. As it can be seen the relative change due to the inclusion of the dynamic terms is substantially independent of the particles filling factor, in this range of concentrations.

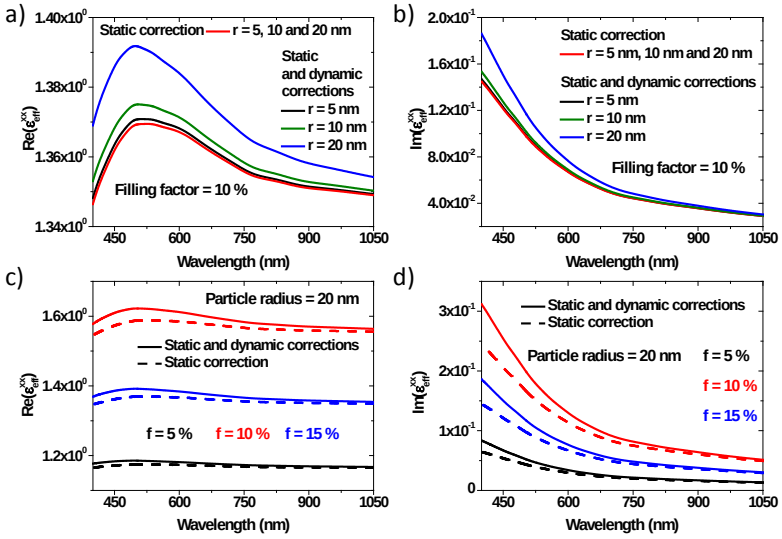

Fig. 4. Real (a) and imaginary (b) part of ε_{eff}^{xx} for a system of Ni spheres embedded in air (the filling factor is 10%), for different values of the particles radius. Real (c) and imaginary (b) parts of ε_{eff}^{xx} for a system of Ni spheres with radius of 10 nm, embedded in air, for different values of the filling factor. All the calculations are performed considering or not the effect of the dynamic term in Eq. (7).

It is clear that for larger particles, as those studied in this work, the dynamic terms play a crucial role. Their relevance in determining the MO response of the magnetoplasmonic systems investigated here will be discussed in the next section.

The last step is to add the glass under-layer and compute the far-field magneto-optical response of the obtained by-layers system using the TMM [37–39], which can generate the reflection and transmission matrices for an arbitrary multilayered system.

#184951 - $15.00 USD Received 5 Feb 2013; revised 13 Mar 2013; accepted 28 Mar 2013; published 12 Apr 2013

3. Comparison with experiments

In this section we compare the theoretical results obtained using our implementation of the LWA method, extended to a general ellipsoid and including MO coupling and the dynamic depolarization term in the polarizability. In order to test our methodology we compare its predictions against the experimental absorption and P-MOKE [65] spectra measured from two types of magnetoplasmonic systems: a set of two samples comprising Ni circular disks of two different diameters (100 and 160 nm), and a sample of Ni disks with elliptical section (in-plane axes of 100 and 160 nm), distributed on a 1 mm thick glass substrate. The samples were grown using the Hole Colloidal Mask Lithography technique [40]. The disks are 30 nm thick for all samples considered and, in the elliptical case, they have the same in-plane orientation. The sizes of the disks are selected to have LPRs in the visible spectral range. In the calculation presented in this section the disks are approximated by oblate ellipsoids and use the disk semi-axes in nm, viz., $a_x = a_y = D/2$ and $a_z = t/2$, where D and t are the diameter and the thickness of the disks, respectively (for the case of elliptical disks the in-plane dimensions are $a_x = D_x/2$ and $a_y = D_y/2$). Note that, since we are in the P-MOKE configuration considering the light impinging perpendicular to the sample surface, i.e., along the *z*-direction parallel to the disks short axis, the only off-diagonal elements different from zero within the dielectric tensor of the single nanoparticle $\tilde{\varepsilon}_2$ are $\pm iQ\varepsilon_2 m_z$.

We start by looking at the set of circular disks of two different diameters. Scanning Electron Microscopy (SEM) investigations of portions of the samples (Fig. 5(a) for D = 100 nm and Fig. 5(b) for D = 160 nm) show that the real diameters of the circular disks for the two samples are D = 95 ± 9 nm and, respectively, D = 160 ± 4 nm. For the embedding medium we use a refractive index n = 1.125 [66].

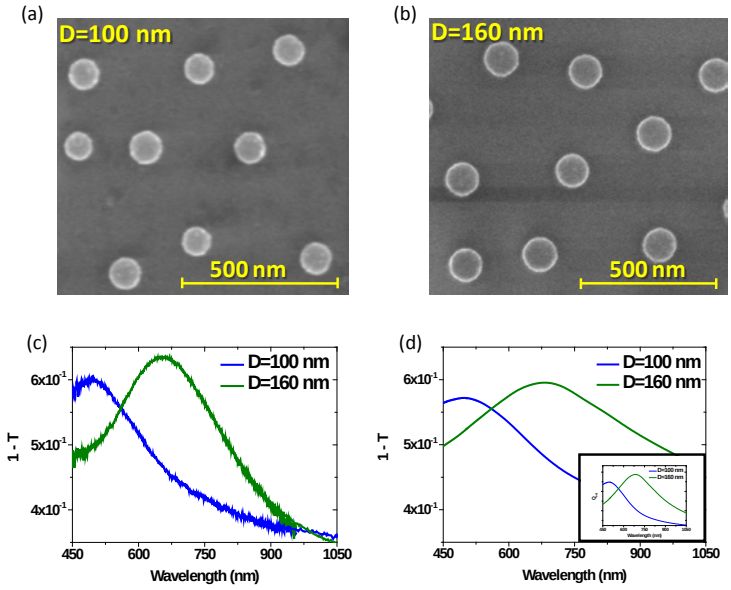

Fig. 5. SEM images of the Ni disks with D = 100 nm (a) and with D = 160 nm (b), on glass substrates, made with Hole Colloidal Mask Lithography technique. The thickness is t = 30 nm. The filling factor can be estimated to be around 13% in both cases. Experimental (c) and calculated (d) absorption spectra, defined as 1 – T, where $T = I_t/I_0$. In the inset it is shown the extinction efficiency Q_{ext} calculated using the imaginary part of the polarizability tensor elements related to the two directions considered.

#184951 - $15.00 USD Received 5 Feb 2013; revised 13 Mar 2013; accepted 28 Mar 2013; published 12 Apr 2013

Figure 5(c) shows the measured absorption spectra $(I_0 - I_t)/ I_0$ of the two sets of Ni circular disks, where I_0 is the intensity of the impinging light and I_t the intensity of the transmitted light. The light was linearly polarized and the measurements were repeated rotating the polarization direction by $\pi/2$ to rule out the presence of optical anisotropy. In Fig. 5(d) we plot the theoretical absorption spectra, obtained using the scattering coefficients calculated with the TMM, viz., 1-T, where T is $|t_{ss}|^2$ or $|t_{pp}|^2$ (with $t_{ss(pp)} = E^t_{s(p)}/E^i_{s(p)}$, the ratio between the transmitted and incident electric fields), depending on the polarization state of the impinging light. The measured and the calculated spectra are in good agreement. The inset in Fig. 5(d) shows the extinction efficiency of a single nanoparticle embedded in air $Q_{ext} \sim k\ \mathrm{Im}(\alpha_{ii})$ [67, 68], with $i = x, y$, using the polarizability tensor elements related to the in-plane axes. It can be seen that the Q_{ext} for the single nanoparticle has a peak due to the excitation of a LPR, which red-shifts increasing the particle volume and whose spectral position coincides with that observed in the measured and calculated absorption spectra. Based on these results we can state that the peak observed in the measured absorption spectra is due to a LPR in the individual nanoparticle, and then any other optical effect, like intrinsic electrostatic resonances [69, 70], can be ruled out. We used the experimentally determined average diameter values to set the length of the semi-axes in the calculations. The calculated spectra agree very well with the measured ones, showing both the characteristic LSPR peak as well as the expected red-shift of the peak position with increasing disk diameter.

We now turn to the magneto-optical response of these disks. We carried out P-MOKE measurements at normal incidence in the visible spectral region, from 440 nm to 750 nm, measuring the complex Kerr angle $\vartheta = \theta + i\varepsilon$, where θ is the Kerr rotation and ε the Kerr ellipticity. An ultra-broadband supercontinuum radiation source coupled with an acousto-optic tunable filter to get monochromatic light, with a resolution of 5 nm, is used. At each wavelength we induced the magnetic saturation of the nanodisks along two opposite directions perpendicular to the sample surface (z-axis) using an external field $|H_z| > |H_s| \sim 2$ kOe. The experimental angles θ' and ε' were measured using the polarization modulation technique [71], which allows the simultaneous measurement of the two Kerr angle components using a photo-elastic modulator and two lock-in amplifiers, one for each component. The Kerr angle components θ and ε are extracted as follows: $2\theta = \theta'(H > H_s) - \theta'(H < -H_s)$ and $2\varepsilon = \varepsilon'(H > H_s) - \varepsilon'(H < -H_s)$. The experimentally retrieved θ and ε are plotted in Fig. 6(a) for the D = 100 nm sample and Fig. 6(b) for the D = 160 nm samples. In both cases, we present the results for *p* and *s* linear polarization states of the incident light. As expected by symmetry, two orthogonal polarizations are equivalent for a circular sample for the experimental geometry utilized here. Indeed, the two experimental spectra recorded with the two polarizations are almost identical. The most salient feature in both sets of spectra is the Kerr ellipticity sign reversal at a wavelength of ~510 nm for the 100 nm diameter disks and of ~690 nm for the 160 nm ones, at which a Kerr rotation maximum is observed, as expected, according to the Kramers-Kronig relations. Comparing to the absorption spectra shown in Figs. 5(c) and 5(d) we note that these features in the Kerr spectra are linked to the excitation of a LSPR in the corresponding set of disks. Indeed, such features are not observed in the P-MOKE spectra of a continuous Ni film, as shown in inset in Fig. 6(f) and therefore they are not due to intrinsic properties of the material. An even more striking evidence is the remarkable agreement between the values of θ and ε found from the experimental measurements (Figs. 6(a) and 6(b)) and the calculated values (Figs. 6(c) and 6(d)) using dielectric optical and MO susceptibilities data sets taken from literature [72, 73]. It is worthy to point out that the agreement is obtained without the need of any adjustable parameters. Not solely the spectral shape of θ and ε is reproduced with a good accuracy, e.g. the wavelength at which ε changes its sign, but also their absolute values are in quantitative agreement with the experimental data.

#184951 - $15.00 USD Received 5 Feb 2013; revised 13 Mar 2013; accepted 28 Mar 2013; published 12 Apr 2013

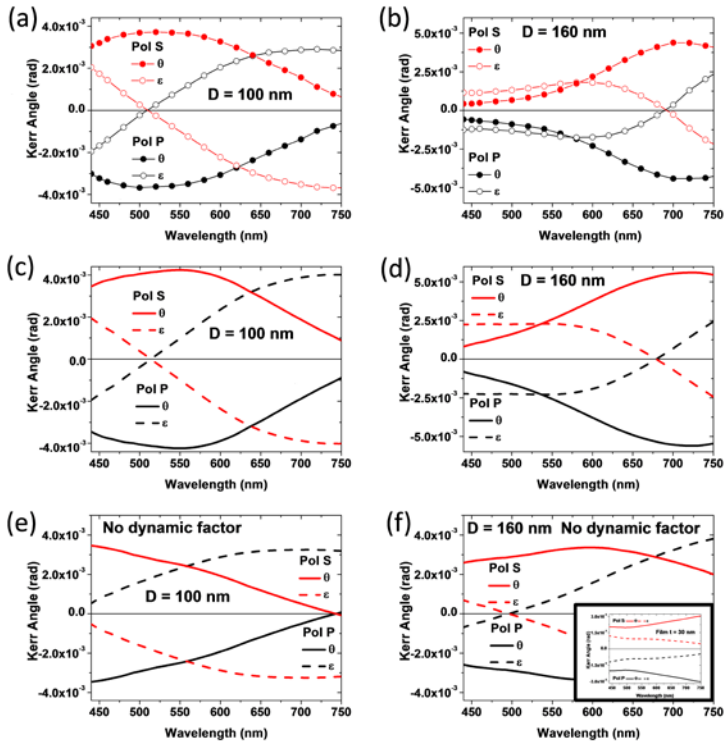

Fig. 6. Experimental Kerr angle in P-MOKE configuration, for (a) D = 100 nm and (b) D = 160 nm. Calculated spectra for (c) D = 100 nm and (d) D = 160 nm. The calculation is performed for the multilayered system air/effective medium/glass, where n_{glass} = 1.5. The effective medium film thickness is 30 nm and the filling factor is f = 13%. Calculated Kerr angle in P-MOKE configuration for (e) D = 100 nm and (f) D = 160 nm, neglecting the dynamic depolarization factor. In the inset of (f) the calculated Kerr spectra in the P-MOKE configuration for a Ni film 30 nm thick.

We conjecture here that the key factor responsible for this surprisingly good agreement between calculated and experimental spectra is the inclusion of the dynamic depolarization term in the polarizability tensor. To prove this, we repeat the calculation of the MOKE spectra shown in Figs. 6(c) and 6(d) including only the contributions to the polarizability due to static and radiative losses, as done so far in the literature for magnetic nanoparticles (see [61, 62, 74].). The result of these calculations is shown in Fig. 6(e) for D = 100 nm and in Fig. 6(f) for D = 160 nm, from which it can be clearly evinced that now the calculated spectra fail to reproduce the features observed in the experiments. This demonstrates, together with the results shown in Figs. 4(a)-4(d), the crucial role of the dynamic depolarization term in order to properly account for both the optical and MO response of dispersed and randomly distributed mixture of non-interacting nanoparticles. Many magnetoplasmonic nanostructures, which belong to this category of systems, are of current and future interest, hence making this formalism a suitable way to describe them.

In order to test the applicability of the method presented in this work to the case of particles with lower symmetry than spheres and disks, we applied our methodology also to the more general case of Ni disks having elliptical section, approximated to general ellipsoids. Their in-plane dimensions are 160 ± 9 nm (major axis) and 100 ± 8 nm (minor axis). A SEM image of a portion of the sample is shown in Fig. 7(a), where it can be also seen that in this case the filling factor is much lower, around 2%.

#184951 - $15.00 USD Received 5 Feb 2013; revised 13 Mar 2013; accepted 28 Mar 2013; published 12 Apr 2013

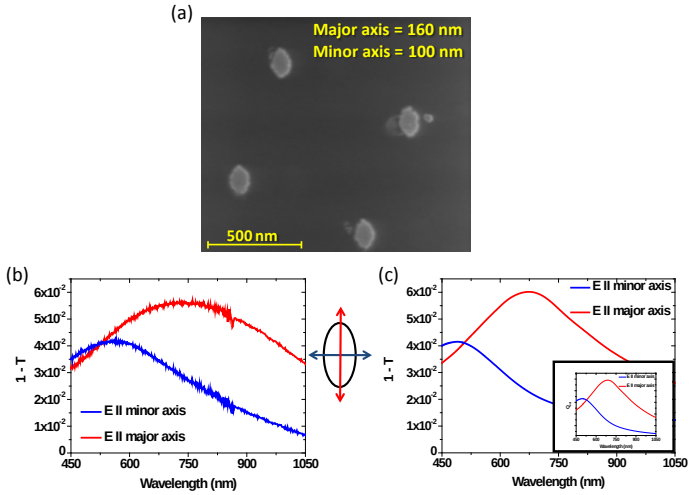

Fig. 7. (a) SEM images of the Ni elliptical disks with D_{long} = 160, D_{short} = 100 nm and t = 30 nm, on glass substrates, made with Hole Colloidal Mask Lithography. It can be seen that the filling factor is around 2%. (b) Experimental and (c) calculated absorption spectra, defined as 1 – T, where T = I_t/I_0. In the inset it is shown the extinction efficiency Q_{ext} calculated using the imaginary part of the polarizability tensor elements related to the two directions considered.

This particles concentration substantially lower than that of the previous samples is accidental and due to the fact that the technique used for the samples nanofabrication does not allow for a very precise control of the filling factor for diluted samples. The absorption spectra of the elliptical disks for the case of linearly polarized light with electric field oscillation direction parallel to the two in-plane principal axes of the elliptical particles are plotted in Fig. 7(b) (experiments) and Fig. 7(c) (calculations). Even in this sample there is a clear evidence of LSPR excitations, although the corresponding absorption peaks are broader than those of the corresponding circular disks, indicating a substantial distribution of particle size in this sample. As expected the LSPR for E parallel to the major axis is red-shifted with respect to the orthogonal polarization state. The agreement between the experimental and calculated spectral positions of the LSPRs is rather good.

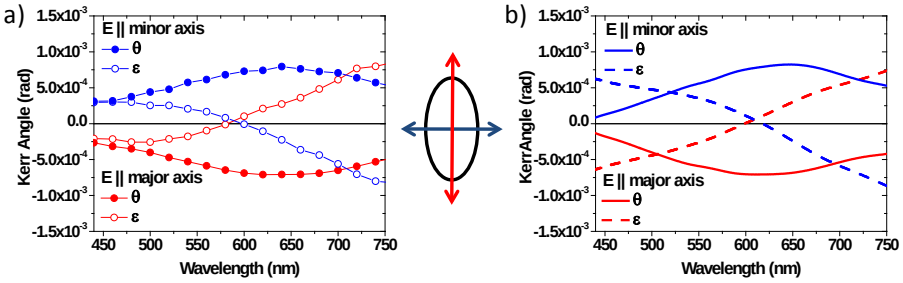

Fig. 8. (a) Experimental and (b) calculated Kerr angle in P-MOKE configuration for the Ni elliptical disks. The calculation is performed for the multilayered system air/effective medium/glass, where n_{glass} = 1.5. The effective medium film thickness is 30 nm and the filling factor is f = 2%.

The comparison between the experimental and calculated P-MOKE spectra is shown in Figs. 8(a) and 8(b), respectively. It is worth noting that the agreement between the results of our modeling approach and the experiments is again remarkable, in particular is much better than the agreement between the calculated and experimental absorption spectra, as if the P-

#184951 - $15.00 USD Received 5 Feb 2013; revised 13 Mar 2013; accepted 28 Mar 2013; published 12 Apr 2013

MOKE measurements were less sensitive to the distribution of particles size. Our calculations reproduce also the slightly different offset in wavelength (≈20 nm) between the ellipticity sign reversal and the rotation maximum observed experimentally upon crossing the polarization of the incoming light.

4. Conclusions

We developed a semi-analytic approach to compute the polarizability tensor of ferromagnetic ellipsoidal particles. Our approach, based on the Long Wavelength Approximation developed by Meier, Wokaun and Liao, has been extended to general ellipsoidal particles $a_x \neq a_y \neq a_z$, with a_x, a_y and a_z the semi-axes of the ellipsoid, including also magneto-optical coupling and dynamic depolarization corrections to account for particles size. The dynamic depolarization corrections are essential in order to well reproduce the experimental spectra, given that the typical sizes of ferromagnetic nanostructures used in most of the experiments conducted in the visible and near infrared spectrum are in the 100 – 300 nm range, viz., exceeding the Rayleigh limit. Furthermore, in order to compare our model outputs against real magneto-optical experiments, measured in reflection geometry and using a large number of particles, we calculated reflectivity spectra using a Maxwell-Garnett Effective Medium Approximation combined with the Transfer Matrix Method. To investigate the prediction of our model, we performed a side-to-side comparison between our calculations and magneto-optical spectra measured in polar configuration on nickel nanodisks deposited on a glass substrate with circular and elliptical shape and sizes of 100 and 160 nm. The disks were modeled as ellipsoids for which the polarizability tensor was computed using our approach. Such disks support localized plasmon resonances in the visible spectrum region, which in turn are responsible for salient spectral features in the magneto-optical spectra. The calculations performed with our formalism are in excellent quantitative agreement with the experimental measurement, with no other parameters than material dielectric optical and magneto-optical constants (taken from literature), and nanostructure sizes and shapes (experimentally determined). We also demonstrated the fundamental role of the dynamic depolarization term when the nanostructure size beyond the Rayleigh limit. This term, often neglected in most of literature magneto-optical studies so far, has to be included in order to obtain realistic approximation of the experimental evidence. Finally, these results demonstrate that our approach, in spite of its approximations, captures the essential physics of the interplay between magneto-optical activity and excitation of localized plasmon resonances in single magnetic nanostructures, optically non-interacting, of broad fundamental and practical interest. For disk-shaped nanostructures, for which our results show that their approximation to ellipsoids works remarkably well, our methodology is accurate and provides an easy alternative to numerical simulations, at least for the case of optical non-interacting magnetoplasmonic particles.

Acknowledgments

N. M., J. B. G-D, A. B. and P. V. acknowledge support from the Basque Government under the Etortek Program IE11-304 and the project PI2012-47 and the Spanish Ministry of Education under the Project No. MAT2012-36844. N. M. and P. V. acknowledge Fabiano Corsetti for the Java applet and Rainer Hillenbrand for valuable discussions. S. B. acknowledges the Knut and Alice Wallenberg Foundation. M. K. and S. v. D. acknowledge support from the National Doctoral Programme in Nanoscience and the Academy of Finland (grant no. 263510). V. B. acknowledges the Göran-Gustafsson Foundation and the Blanceflor Boncompagni-Ludovisi Foundation. J. N. acknowledges the Generalitat de Catalunya under the project 2009-SGR-1292 and the Spanish Ministerio de Economía y Competitividad under the project MAT2010-20616-C02. A. D. and Z. P. acknowledge support from the Swedish Research Council and Swedish Foundation for Strategic Research (Framework program Functional Electromagnetic Metamaterials, project RMA08).

#184951 - $15.00 USD Received 5 Feb 2013; revised 13 Mar 2013; accepted 28 Mar 2013; published 12 Apr 2013